Proc. Natl. Acad. Sci. USA
Vol. 88, pp. 4631–4635, June 1991
Biophysics

Computation of ionic distributions around charged biomolecular structures: Results for right-handed and left-handed DNA

(polyelectrolytes/DNA polymorphism/potentials of mean force)

REINHARD KLEMENT, DIKEOS M. SOUMPASIS, AND THOMAS M. JOVIN

Max-Planck-Institut für Biophysikalische Chemie, Abteilung Molekulare Biologie, Am Fassberg, W-3400 Göttingen, Federal Republic of Germany

Communicated by Manfred Eigen, December 26, 1990

ABSTRACT **We introduce an efficient computational methodology employing the potentials of mean force approach for estimating the detailed three-dimensional ionic distributions around arbitrarily complex charged biomolecular structures for all monovalent salt concentrations of practical interest (e.g., 0.1–5.0 M NaCl). Such distributions are required for specifying thermodynamic and structure-specific features of ion-mediated interactions of charged proteins, DNA and RNA, membranes, and macromolecular assemblies. As a first application, we present results for distributions around the B and Z_I conformers of the DNA oligomer $d(C\text{-}G)_{18}\cdot d(C\text{-}G)_{18}$. The ionic microenvironment depends strongly on the DNA conformation, sequence, and bulk salt concentration.**

The computation of ionic distributions around highly charged biomolecules has been a subject of continuous interest for the past 20 years due to the importance of the ionic environment for structural stability and transitions as well as for intermolecular interactions and binding equilibria. For example, in the case of DNA, ionic effects play a central role in the extensively studied B → Z transition (for recent reviews, see refs. 1 and 2), at all levels of DNA structural organization (refs. 3 and 4 and references therein), and in ligand–DNA binding equilibria (5).

The approaches proposed to date for computing ionic distributions around DNA vary widely with respect to (*i*) the structural modeling of the DNA–water–ions system, (*ii*) the statistical approximations employed, (*iii*) the computational complexity, (*iv*) the range of bulk ionic concentrations, and (*v*) the DNA conformations studied. If the water, ions, and DNA components are described microscopically, the only currently feasible way to determine ionic distributions is by large-scale computer simulations (i.e., Monte Carlo and molecular dynamics), as reported by Clementi and Corongiu (6–8) and more recently by van Gunsteren *et al.* (9). These calculations are extremely costly and can only be performed practically in the absence of added salt. For example, to simulate a 0.1 M NaCl electrolyte around DNA, one has to consider at least 50 anion–cation pairs and 25,000 water molecules in the central simulation box, an effort that is at present impossible.

In previous studies water has been represented as a dielectric continuum and the ions have been considered either as hard or soft spheres or simply point particles. The treatments have substantial differences in the structural modeling of DNA and the use of statistical approximations. If one pictures a DNA structure as an infinitely long uniformly charged cylinder, it is straightforward to compute the average cylindrically symmetric ionic distributions through the numerical solution of the Poisson–Boltzmann (10–12) and hypernetted chain equations (13, 14) as well as by the Monte Carlo technique (14, 15). However, all the essential local sequence and conformation-dependent variations in the distributions are lost. During the past 6 years, it became possible to solve the Poisson–Boltzmann equation for more realistic structural models of DNA structures (16, 17) but, due to numerical convergence problems, the range of salt (NaCl) concentrations over which the distributions can be obtained (at great computational cost) is rather limited and does not include the high salt regime where both salt-induced DNA transitions (B → Z and B → A) and many protein–DNA dissociation equilibria take place. In addition noncoulombic core repulsions are usually ignored in Poisson–Boltzmann studies. Finally, a recent approach (18) based on the reference interacting sites model theory and realistic DNA modeling is useful only for infinite straight periodic DNA and cannot be used for more complex irregular structures (e.g., curved DNA, hairpins, cruciforms, tRNA, etc.). Furthermore, this formalism does not appear to work at less than 2 M NaCl due to numerical convergence problems and is computationally expensive.

This brief overview clearly shows that a general, fairly accurate, computationally efficient method to approximately solve the problem at hand for arbitrarily complex biomolecular structures over a wide range of bulk ionic concentrations is highly desirable but has been previously unavailable. We present here an approach based on the potentials of mean force framework (19–21) that emphasizes the role of realistic structural modeling and effective ionic interactions and has been found to describe simple salt effects on DNA structure and structural transitions very well (19–25). This method combined with force fields describing intramolecular interactions provides a general formalism for modeling biomolecules in simple electrolyte solutions (24, 25). We have used it to calculate ionic distributions around DNA immersed in simple electrolytes.

Theoretical Background

Consider a homogeneous multicomponent electrolyte consisting of m ionic species α_i, $i = 1, \ldots, m$ in water, with bulk number densities $\rho_i^0 = N_i/V$. N_i is the number of ions of type α_i and V the volume. $N = \Sigma_i N_i$ is the total number of ions present in the system.

Fixing any n ions of types α_i (abbreviated $\{\underline{\alpha}\}$) at positions $\vec{R}_1, \ldots, \vec{R}_n$ (abbreviated $\{\vec{R}\}$) generates an external field coupling to the remaining $N - n$ mobile ions, which gives rise to a set of m spatially dependent ionic distributions around the configuration $\{\vec{R}\}$. They are denoted $\rho_i(\vec{x} \mid \{\vec{R}, \underline{\alpha}\})$ and correspond to the conditional probability density of finding an ion of type α_i at a position $\vec{x}$, given that the set $\{\underline{\alpha}\}$ of n fixed ions is in configuration $\{\vec{R}\}$. That is,

$$\rho_i(\vec{x} \mid \{\vec{R}, \underline{\alpha}\}) = \frac{\rho^{(n+1)}(\vec{x}, \{\vec{R}\})}{\rho^{(n)}(\{\vec{R}\})}, \qquad [1]$$

The publication costs of this article were defrayed in part by page charge payment. This article must therefore be hereby marked "*advertisement*" in accordance with 18 U.S.C. §1734 solely to indicate this fact.

where $\rho^{(n+1)}$ and $\rho^{(n)}$ are the $n+1$ and n particle distributions' functions of the homogeneous electrolyte comprising all N ions, respectively (for definitions and properties, see refs. 26 and 27). Eq. 1, which is simply a Bayes formula, is very general and applies irrespective of the specific model adopted to describe the aqueous electrolyte, the number of ionic species involved, and the statistical mechanical approximations used to cope with the many-body problem.

If one now identifies the n fixed ions with the n charged sites of a given biomolecular structure in solution, Eq. 1 becomes a feasible route for numerical computation of the three-dimensional ionic distributions around the structure, provided one adopts several approximations both at the modeling and the statistical averaging levels. These are absolutely required due to the horrendous complexity of the system (biomolecule–water–ions) considered.

From now on, we specialize the treatment to the concrete case of a DNA fragment in a simple electrolyte (e.g., water–NaCl) and denote the two ionic distributions to be determined $\rho_2(\vec{x} \mid \{\vec{R}, \underline{\alpha}\})$ (index 2, cations) and $\rho_1(\vec{x} \mid \{\vec{R}, \underline{\alpha}\})$ (index 1, anions). By using the Kirkwood superposition approximation (26) to decompose the many particle correlations entering Eq. 1, one obtains

$$\rho_i(\vec{x} \mid \{\vec{R}, \underline{\alpha}\}) = \rho_i^0 \prod_{k=1}^{n} g_{ik}(|\vec{x} - \vec{R}_k|) \quad i = 1, 2, \qquad [2]$$

where k refers to the kth charged site of DNA at position $\vec{R}_k$ and with charge q_k. The approximate formula (Eq. 2) (which becomes exact far away from the structure) now involves only the ionic pair correlation functions g_{ik} that depend solely on the distances $|\vec{x} - \vec{R}_k|$ and the thermodynamic state parameters (i.e., the temperature T, the bulk densities ρ_i^0, and the external pressure). These quantities can be determined presently neither from experiments (e.g., neutron scattering) nor from supercomputer simulations (Monte Carlo or molecular dynamics) of models describing the water component at the microscopic level. For this reason they are calculated in the context of the most widely studied McMillan–Mayer (i.e., solvent averaged) level model of electrolytes, which is the restricted primitive model (28) in which the ions are pictured as charged hard spheres of diameter σ and water is a dielectric continuum of dielectric constant $\varepsilon = 78.4$ at 298.14 K. In addition, we adopt the statistical approximations involved in the exponential mean spherical approximation (29, 30) treatment of the restricted primitive model that yields essentially closed form expressions for the g_{ik} (for technical details, see ref. 19 and especially ref. 25). Alternatively, one could use the more accurate hypernetted chain or Monte Carlo $g(r)$ values. A detailed formal analysis of the proposed methodology will be published elsewhere.

Procedure

All ionic distribution calculations reported herein were carried out on a 36-base-pair long DNA structure consisting of the d(C-G)$_{18}$·d(C-G)$_{18}$ duplex in the B and Z_I conformation at various bulk salt concentrations in the range of 0.01–5 M. The probability densities were calculated on both a cylindrical and a cartesian grid. The two grid geometries were chosen to emphasize different views of the density distribution. The cartesian grid yields good results for contour plots, whereas the cylindrical grid reflects the shape of the DNA structures and has a higher grid point density close to the molecule, where the strongest changes in the distribution are found. Both volumes were sampled with the same number of grid points ($50 \times 50 \times 50$). The cartesian grid dimensions were $40 \times 40 \times 40$ Å with a grid constant of 0.8 Å. The cylindrical grid had a height of 40 Å and a radius of 50 Å with an angle increment $\Delta\phi = 7.2°$ between two adjacent rays extending outward from the center. Only the central portion (roughly one helical turn) of the 36 base pairs was enclosed by the integration volume to exclude end effects.

As in previous work (19–25), the distance of closest approach of an ion pair σ was set to 4.9 Å and the bulk dielectric constant was that of water ($\varepsilon_w = 78.4$). A cutoff of 35 Å was imposed on the potential of mean force interaction. The formal charge of $-72\,e$ of the structures was assumed to be shared by all atoms of the molecule; i.e., we used the partial charge parametrization of the AMBER program (31, 32). On each grid point outside the DNA structures, that is, at a minimal distance σ away from the surface, a test charge of 1 e (+ for cations and − for anions) was placed and the local ionic probability densities were calculated using Eq. 2. The calculations were carried out on an IBM model 3090-300 main frame computer and the average central processing unit time required to calculate the full three-dimensional cation and anion distributions around one structure (1662 atoms and 125,000 grid points) for one single bulk density was about 11 min. The color contour plots of the ion distributions were generated with the TCL-Image program (Delft Center for Image Processing; Multihouse, Amsterdam) and the SCHAKAL program (E. Keller, University of Freiburg, F.R.G.) was used to draw the space-filling DNA structures.

Results and Discussion

For each salt concentration and structure, the total output of the computation consists of a field of 125,000 probability density values per ionic species. Once these values are known, all other quantities or representations of interest (e.g., contour plots in selected cross-sections, charge densities, electrostatic potentials and fields, cylindrically averaged distributions, etc.) can be obtained using standard computational methods. After some experimentation, we have found that color-coded contour plots are most convenient for communicating major features of the informational product of the computations. The probability densities shown here were normalized relative to the bulk salt concentration ρ_0; i.e., $\bar{\rho}(\vec{r}) = \rho(\vec{r})/\rho_0$. The color contour plots depict cross-sections at the center of the cartesian integration box in the x–y and y–z planes. The B and Z_I structures are shown at the center of these plots. The black regions at the center of the plots, close to the DNA structures, denote areas not accessible to the ions due to their hard core exclusion.

In Fig. 1 we show y–z and x–y contours of the cationic (Na^+) probability density distribution around the B and Z_I forms of d(C-G)$_{18}$·d(C-G)$_{18}$ at 0.1 M NaCl bulk concentration. [The z axis is the helix axis and the DNA atomic coordinates are those of Arnott and Hukins (33) and Wang et al. (34).] In Fig. 1 *Lower*, only the central x–y cross-sections are shown, corresponding to two base pairs.

In the B form, the highest cationic density regions (red → yellow) are found to be in the major and minor grooves, with a strong maximum in the major groove. At a distance of about 17 Å from the helix axis, the distribution becomes radially symmetric and is no longer influenced by the structural details of the DNA conformation. For the Z_I form the cations are concentrated on one side of the DNA structure toward the deep minor groove. The ionic distribution is more asymmetric compared to that of B DNA (Fig. 1 *Left*) because of the phosphate group geometry. For both structures the integration volume is essentially free of anions at a 0.1 M salt concentration.

The ionic distributions change dramatically as one increases the bulk salt concentration to 5.0 M (Fig. 2). Many-body packing effects due to the finite size of the hydrated ions become as important as Coulomb screening and give rise to regions of low cationic densities (dark blue part of the color

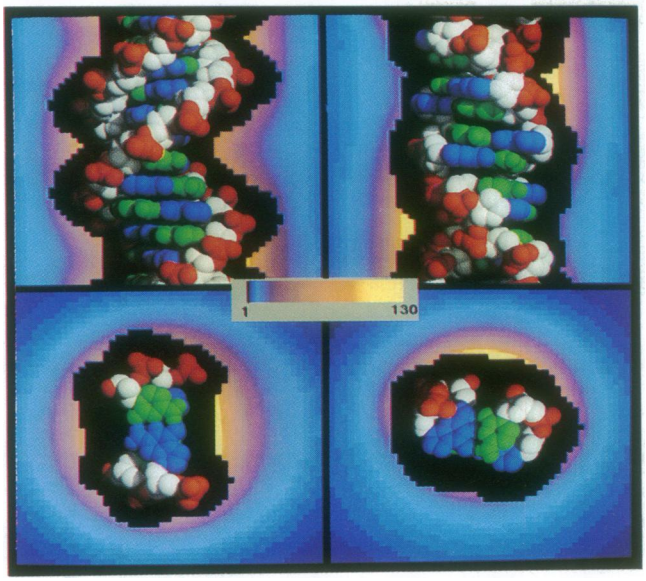

FIG. 1. Normalized distribution of cations (Na^+) around the central 12 base pairs of B (*Left*) and Z_I DNA (*Right*) at 0.1 M bulk salt. (*Upper*) *y–z* cross sections at the center of the integration volume that coincides with the helical axis of the DNA structures. (*Lower*) Associated *x–y* cross sections located between the central base pairs. The dimensions of the cross sections are 40 × 40 Å. The DNA structures are shown as space-filling models at the center of the pictures [color coding: blue, guanine; green, cytosine; white, sugar; red, phosphates (including O3′ and O5′)]. The black areas close to the structures are free of ions due their finite size. The scale of the color contours is shown at the center with the minimum and maximum values indicated. The groove regions show highest probabilities for both structures (see text for more details).

scale) intermixed with regions of bulk (light blue) and islands of high cationic density (red → yellow scale). For B DNA, the high probabilities in the major and minor groove of the *x–y* cross-section have disappeared, and instead one finds two high-probability islands between two phosphate groups. In the immediate vicinity of the molecule, the distribution becomes highly structured and, as indicated by the color scale, there exist regions where the local density drops below the bulk salt concentration (dark blue areas). For the Z_I conformer (*Right*), the ionic atmosphere becomes highly structured as well and the highest probabilities coincide with the sites on the DNA bearing the highest charge, i.e., the phosphates.

In Fig. 3 we compare the ionic microenvironment of the two DNA conformations at 5.0 M NaCl in a different way. The *x–z* and *x–y* cross-sections are exactly as in Figs. 1 and 2 but the quantity color coded is the difference between the local cationic and anionic densities, a quantity proportional to the local net charge density. Yellow and orange code for regions where the charge density is positive (excess of cations) whereas light and dark blue code for negative charge density (excess of anions) and dark grey codes for zero net charge density. The complex layered structure and conformation dependence of the charge distributions are particularly clear in this representation. The different domains of net charge in the vicinity of the B form are well separated, with a layer of net positive charge at the contact surface and a layer of net negative charges behind it separated by a neutral domain. This shell of net negative charge is due to the neutralization of the DNA charge distribution by the first layer of ions and the excess of cations in the second layer (see also Fig. 4 *c* and *d*). At the contact surface of Z_I DNA, both net positive and net negative domains coexist, a circumstance not observed in the B form. Negative patches are found in the shallow major groove just over the CpG step. This region of an excess negative charge coincides with locations at which Cl^- ions have been found in Z DNA crystal (35). The net positive charge domains in Z_I DNA are correlated with the phosphate groups, where the highest probability densities are found between adjacent intrastrand groups.

The cylindrically averaged and normalized cationic and anionic probability densities [$\bar{\rho}(R) = \rho(R)/\rho_0$] around the B and Z_I forms are depicted as function of the radial distance from the helix axes in Fig. 4. We also include the fractional charge neutralization calculated by integrating the radial

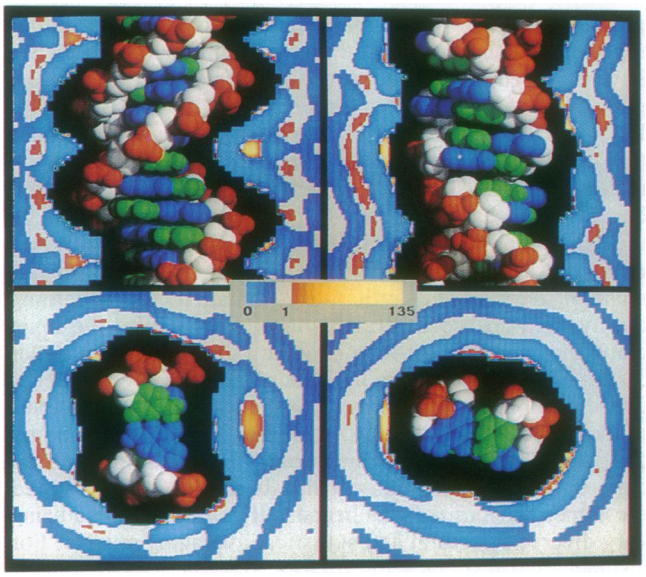

FIG. 2. Cation distributions around B and Z_I DNA at 5.0 M NaCl. The environment of both conformations becomes more structured and looks somewhat patchy. Due to packing effects, the cations form layers around the structures. As indicated by the color scale, one can find regions (blue areas) where the local density drops below the bulk salt concentration (gray color). Areas with highest probability are found between the phosphate groups. Other details are as in Fig. 1.

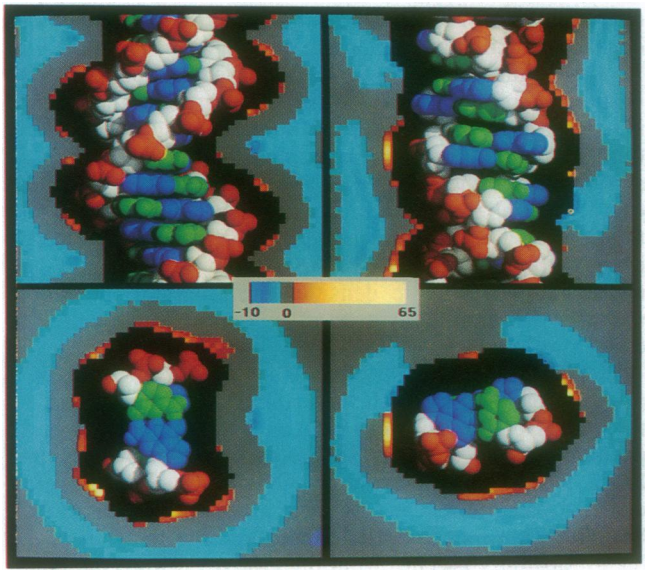

FIG. 3. Net charge density $(\rho^+ - \rho^-)/\rho_0$ around B and Z_I DNA at 5.0 M salt. Blue regions show a negative charge excess, red regions show positive charge excess, and the gray regions are neutral (see color scale for normalized values). For the B form positive and negative regions are separated by a neutral layer and at the contact surface we find only a positive charge excess, whereas for the Z_I form both positive and negative regions are found at the contact surface.

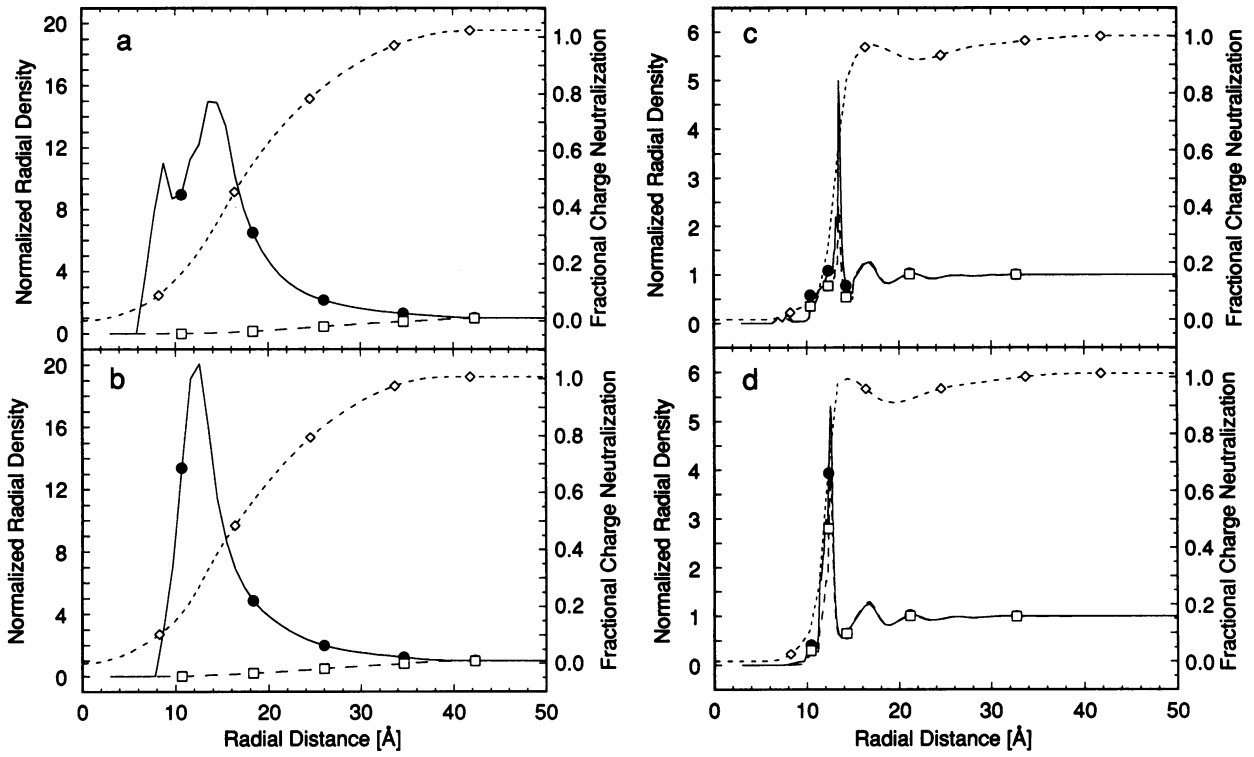

FIG. 4. Normalized radial densities and fractional charge neutralization around the B and Z_I structures as a function of the distance perpendicular to the helix axis. (*a* and *b*) Densities (●, cations; □, anions) and fractional charge neutralization (◇) around B DNA (*a*) and Z_I DNA (*b*) at 0.1 M NaCl. The anion curves vary between 0 and 1 and indicate that the integration volume is practically free of anions. (*c* and *d*) Densities and fractional charge neutralization around B DNA (*c*) and Z_I DNA (*d*) at 5.0 M NaCl (symbols are as in *a* and *b*).

density distributions for cations and anions and normalizing by the total amount of molecular charge in the integration volume. A value of one corresponds to 100% neutralization of the DNA charge by the ionic cloud. At low salt (0.1 M NaCl), the radial cationic distribution curves for the B and Z_I form decay rapidly beyond the positions of the phosphate groups plus the distance of closest approach σ ($\approx$15.5 Å for B and $\approx$12.6 Å for Z_I). Between 5 and 15 Å, the distribution curve for B DNA exhibits a peak due to the high probability densities found in the major and minor groove (see also Fig. 1). This feature is missing for the Z_I structure, because of the shallow major groove and the deep narrow minor groove that is not accessible to hydrated sodium ions. Since Z_I DNA is thinner than B DNA, the maximum of the distribution is shifted toward the helix axis. The graphs for the fractional charge neutralization exhibit a similar behavior for the B and the Z_I structures. In both cases 70% of the molecular charge is neutralized at a distance of $\approx$20 Å from the helix axis. The curves for the anionic densities indicate that the model volumes are essentially free of anions at this electrolyte concentration.

The high salt radial distributions (Fig. 4 *c* and *d*) show a pronounced peak for both the cation and anion densities at the radius of the contact surface. Due to the many-body packing effect of the hard sphere potential, anions are also found in the integration volume and contribute to the overall distribution pattern. The structured groove region for B DNA has almost disappeared as a consequence of the shift of the high-probability patches from the grooves toward the phosphate groups (see also Fig. 2). The difference in the distribution patterns of B and Z_I DNA, mentioned above and shown in Figs. 2 and 3, is reflected in the difference between the first peak of cationic and anionic distributions. With Z_I DNA, both cations and anions are found with high probability at the contact surface (see also Fig. 3), whereas with the B form, the cations are predominant. The overall shape of the distribution curves reflects the packing effects known to occur in dense fluids; i.e., cations and anions form shells around the molecular structure. Practically all DNA charge is neutralized by the first layer of ions, as indicated by the fractional charge density. The dip in the fractional neutralization curve is caused by the excess of anions in the second ion shell.

A detailed quantitative comparison of the present work to previous studies is impossible at present. None of the studies reported to date covers the range of salt concentrations we have explored, and except for two cases (16, 17) the papers published were concerned exclusively with the B form of DNA modeled as an unstructured infinite charged cylinder (12–15). For the Poisson–Boltzmann treatments based on realistic B DNA structural models similar to that presented here (16, 17), quantitative results comparable, for example, to the cylindrically averaged distributions given in Fig. 4 *a* and *c* are not available. However, all studies reported so far, including ours, yield quantitatively similar results concerning the average charge neutralization of B DNA by the ionic cloud that is essentially complete at a distance on the order of 20–30 Å from the helix axis depending on the bulk concentration. This is simply a consequence of the principles of local electroneutrality and screening that are valid in any charged system. The cylindrically averaged normalized counterion probability density distribution $\rho_+(R)/\rho_0$ is suited for numerical comparisons because it can be obtained using very diverse structural and statistical averaging models. For instance, at 0.1 M NaCl and B DNA, the charged cylinder by the Poisson–Boltzmann analysis, by the hypernetted chain analysis, and by the present study predict maximal ρ_+/ρ_0 values of 54 (23), 21 (13), and 15, respectively. The Poisson–Boltzmann value is too high due to the neglect of ion–ion core repulsions and ionic correlations. The smaller discrepancy between the present study and the hypernetted chain study is due to the different structural modeling and statistical me-

chanical approximations (hypernetted chain versus Kirkwood superposition approximation) used to treat the many-body problem.

Concluding Remarks

The approximate method we presented above permits the fairly accurate estimation of the three-dimensional ionic distributions around arbitrarily complex charged biomolecular structures for all bulk ionic concentrations of practical interest. It is computationally robust and economic (10^3 to 10^4 times faster than Monte Carlo and molecular dynamics simulations for the same model) and can also be extended to the case of ionic mixtures (e.g., $MgCl_2$–NaCl) described at the charged hard sphere level. A further important advantage is that the ionic probability density at a given point of interest (e.g., in front of a reactive site) can be directly computed without first solving nonlinear differential or integral equations everywhere around the structure, as is the case for the Poisson–Boltzmann, hypernetted chain, and reference interacting sites model approaches. In collaboration with A. C. Garcia (Los Alamos National Laboratory), we have performed an extensive Monte Carlo study over a wide range of salt concentrations of the ionic distributions around a simpler DNA structural model consisting of the phosphate groups alone to test the method used here. Overall, the agreement between the two methods is very good except for the fact that very close to the structure the Monte Carlo radial distributions at high salt concentrations are 20–30% lower than those obtained using the present technique. (A detailed account of this comparative study will be published elsewhere.) This behavior is expected because (*i*) the exponential mean spherical approximation pair correlation function currently implemented, bound the true $g(r)$ values from above and (*ii*) the Kirkwood superposition approximation overestimates the correlations of particles very close to each other.

We emphasize the generality of the approach. That is, any macromolecular structure for which the three-dimensional distribution of charged and other solvent-accessible atoms is known experimentally (e.g., from crystallographic or NMR analysis) or derived theoretically can be accommodated. Specific binding sites involved in regulation, catalysis, and transport, as well as packing and aggregation phenomena, are of particular interest. The potential of mean force formalism provides a unique means for estimating the overall thermodynamic properties (21, 23) and the local structural features of such complex systems.

We thank Dr. A. E. Garcia for many discussions and collaborations. This research was supported by the Max Planck Society and the German Ministry of Science and Technology (Bundesministerium für Forschung und Technologie; Sonderforschungsschwerpunkt Bioprozesstechnik).

1. Jovin, T. M., Soumpasis, D. M. & McIntosh, L. P. (1987) *Annu. Rev. Phys. Chem.* **38,** 521–560.
2. Soumpasis, D. M. & Jovin, T. M. (1987) in *Nucleic Acids and Molecular Biology,* eds. Eckstein, F. & Lilley, D. M. J. (Springer, Berlin), pp. 85–111.
3. Soumpasis, D. M. (1986) in *Biomolecular Stereodynamics IV,* eds. Sarma, R. H. & Sarma, M. H. (Adenine, Guilderland, NY), pp. 47–61.
4. Record, T. M., Jr., Mazur, S. J., Melancon, P., Roe, J. H., Shanes, S. L. & Unger, L. (1981) *Annu. Rev. Biochem.* **30,** 997–1021.
5. Record, T. M., Jr., Anderson, C. F. & Lohman, T. M. (1978) *Q. Rev. Biophys.* **11,** 103–178.
6. Clementi, E. & Corongiu, G. (1981) *Biopolymers* **20,** 551–571.
7. Clementi, E. & Corongiu, G. (1981) *Biopolymers* **20,** 2427–2483.
8. Clementi, E. & Corongiu, G. (1982) *Biopolymers* **21,** 763–777.
9. van Gunsteren, W. F., Berendsen, H. J. C., Geurtsen, R. G. & Zwinderman, H. R. J. (1986) *Ann. N.Y. Acad. Sci.* **482,** 297–363.
10. Stigter, D. S. (1975) *Colloid and Inter. Sci.* **53,** 296–306.
11. Gueron, M. & Weisbuch, G. (1980) *Biopolymers* **19,** 353–382.
12. Le Bret, M. & Zimm, B. H. (1984) *Biopolymers* **23,** 287–312.
13. Bacquet, R. & Rossky, P. J. (1984) *J. Phys. Chem.* **88,** 2660–2669.
14. Murthy, C. S., Bacquet, R. J. & Rossky, P. J. (1985) *J. Phys. Chem.* **89,** 701–710.
15. Mills, P., Anderson, C. F. & Record, T. M., Jr. (1985) *J. Phys. Chem.* **89,** 3984–3994.
16. Pack, G. R. & Klein, B. J. (1984) *Biopolymers* **23,** 2801–2823.
17. Yayaram, B., Sharp, K. A. & Honig, B. (1988) *Biopolymers* **28,** 975–993.
18. Hirata, F. & Levy, R. M. (1989) *J. Phys. Chem.* **93,** 479–484.
19. Soumpasis, D. M. (1984) *Proc. Natl. Acad. Sci. USA* **81,** 5116–5120.
20. Soumpasis, D. M., Wiechen, P. & Jovin, T. M. (1987) *J. Biomol. Struct. Dyn.* **4,** 535–552.
21. Soumpasis, D. M., Garcia, A. E., Klement, R. & Jovin, T. M. (1991) in *Theoretical Biochemistry and Molecular Biophysics,* eds. Beveridge, D. L. & Lavery, R. (Adenine, Guilderland, NY), Vol. 1, pp. 343–360.
22. Soumpasis, D. M., Robert-Nicoud, M. & Jovin, T. M. (1987) *FEBS Lett.* **213,** 341–344.
23. Soumpasis, D. M. (1988) *J. Biomol. Struct. Dyn.* **6,** 563–574.
24. Garcia, A. E. & Soumpasis, D. M. (1989) *Proc. Natl. Acad. Sci. USA* **86,** 3160–3164.
25. Klement, R., Soumpasis, D. M., von Kitzing, E. & Jovin, T. M. (1990) *Biopolymers* **29,** 1089–1103.
26. Hill, T. L. (1962) *An Introduction to Statistical Thermodynamics* (Addison & Wesley, Reading, MA).
27. Hansen, J. P. & McDonald, J. R. (1976) *Theory of Simple Liquids* (Academic, London).
28. Friedman, H. L. & Dale, W. D. (1977) in *Statistical Mechanics A: Equilibrium Techniques,* ed. Berne, B. J. (Plenum, NY), pp. 85–134.
29. Anderson, H. C. & Chandler, D. (1972) *J. Chem. Phys.* **57,** 1918–1929.
30. Anderson, H. C., Chandler, D. & Weeks, J. D. (1972) *J. Chem. Phys.* **57,** 2626–2631.
31. Weiner, P. K. & Kollman, P. A. (1981) *J. Comput. Chem.* **2,** 287–303.
32. Weiner, P. K., Kollman, P. A., Cuse, U. C., Singh, C., Ohio, G., Alogerma, S., Profeta, J. R. & Weiner, P. (1984) *J. Am. Chem. Soc.* **106,** 765–784.
33. Arnott, S. & Hukins, D. W. L. (1972) *Biochem. Biophys. Res. Commun.* **47,** 1504–1509.
34. Wang, A. H., Quigley, G. J., Kolpak, F. J., van der Marel, G., van Boom, J. H. & Rich, A. (1981) *Science* **211,** 171–176.
35. Drew, H., Takano, T., Tanaka, S., Itakura, K. & Dickerson, R. E. (1980) *Nature (London)* **286,** 567–573.